Integrated nanoscale silicon sensors using top-down fabrication

O. H. Elibol, D. Morisette, D. Akin, J. P. Denton, and R. Bashir[a]
Laboratory of Integrated Biomedical Micro/Nanotechnology and Applications,
Birck Nanotechnology Center, School of Electrical and Computer Engineering, Department of
Biomedical Engineering, Purdue University, West Lafayette, Indiana 47907

Semiconductor device-based sensing of chemical and biological entities has been demonstrated through the use of micro- and nanoscale field-effect devices and close variants. Although carbon nanotubes and silicon nanowires have been demonstrated as single molecule biosensors, the fabrication methods that have been used for creating these devices are typically not compatible with modern semiconductor manufacturing techniques and their large scale integration is problematic. These shortcomings are addressed by recent advancements in microelectronic fabrication techniques which resulted in the realization of nanowire-like structures. Here we report a method to fabricate silicon nanowires at precise locations using such techniques. Our method allows for the realization of truly integrated sensors capable of production of dense arrays. Sensitivity of these devices to changes in the ambient gas composition is also shown. © *2003 American Institute of Physics.* [DOI: 10.1063/1.1630853]

Miniaturization of biological and chemical analysis tools to the level of the ''lab on a chip'' decreases the analysis time and the sample size needed for specific detection in genomic and proteomic applications as well as in detection of warfare agents and environmental pollutants. In general, as the sensor dimensions shrink down to the size of the analyte, the sensitivity of the device increases. Specifically, nanowire type sensors are very attractive because their large surface area to volume ratio results in high sensitivity. Carbon nanotubes[1] and silicon nanowires[2] have been demonstrated as single molecule biosensors, but the fabrication methods that have been used for creating these devices are typically not compatible with modern semiconductor manufacturing techniques and their large scale integration is quite problematic.[3] These shortcomings are addressed by recent advancements in microelectronic fabrication techniques which resulted in the realization of nanowire-like structures.[4,5] Here we describe a fabrication method and initial test results on a silicon nanowire sensor that is realized using top-down microelectronics processing techniques. A process known as confined lateral selective epitaxial growth (CLSEG)[5] was utilized to obtain single crystal silicon nanoplates that are as thin as 7 nm and nanowires as small as 40 nm in diameter at precise locations. The method allows for the realization of truly integrated dense array of sensors. Initial testing of the devices showed sensitivity towards oxygen ambient, suggesting the possibility of using these sensors for chemical and biological detection.

Fabrication of the devices was performed on p-type low doped silicon wafers. A 2000-Å-thick oxide was grown by wet oxidation for substrate isolation. A sacrificial layer of amorphous silicon with 100 Å of thickness was deposited and defined lithographically on the silicon dioxide layer [Fig. 1(a)]. Another 4000-Å-thick oxide layer was deposited using plasma enhanced chemical vapor deposition (PECVD). Via

holes that will subsequently be filled with silicon and act as the source and drain regions were etched using a reactive ion etch [Fig. 1(b)]. The sacrificial layer of polycrystalline silicon was removed selectively by wet etching using tetramethyl-ammonium-hydroxide. The removal of the sacrificial layer defines a gap between the thermally grown oxide and deposited oxide. Due to the surface tension of the liquid after the rinse step, a bridge formed by the top oxide collapsed, leaving via holes near the anchors of the oxide bridge [Fig. 1(c)]. These via holes were used as a mold for the epitaxial silicon to grow through which would later form the nanowires. A seed hole was wet etched in the thermal oxide on the source side down to the silicon surface [Fig. 1(d)] in order to grow epitaxial silicon by CLSEG with no intentional doping. This process yields good quality single crystal silicon with low n-type doping ($\sim 10^{16}$ cm^{-3}). Epitaxial silicon grows through the via holes at the edges of the collapsed oxide bridge as well as at the interface of the collapsed region. The silicon grown in this region forms a 6–7-nm-thick plate. The excess silicon remaining on the surface was removed by chemical-mechanical polishing [Fig. 1(e)]. A high dose n-type blanket implant was performed in order to form conductive source and drain regions. After depositing a 2000-Å-thick PEVCD oxide insulation layer, a high temperature anneal is performed to activate and drive in the implanted dopant, and to densify the PECVD oxide. Contact holes were then wet etched in the oxide to access the silicon source and drain regions. A 200 Å of chromium, followed by 2500 Å of gold was evaporated and patterned to define electrical contacts [Fig. 1(e)].

The final step in the fabrication process was to uncover the silicon nanowires by removing the encapsulating oxide by unpatterned wet etching in buffered hydrofluoric acid (BHF) [Fig. 1(f)]. The fabrication method yields a film of silicon about 7 nm thick in the collapsed regions, and 50 nm diameter wires at the edges of the film between the anchors. Etching in BHF for 6 min removes the oxide covering on the

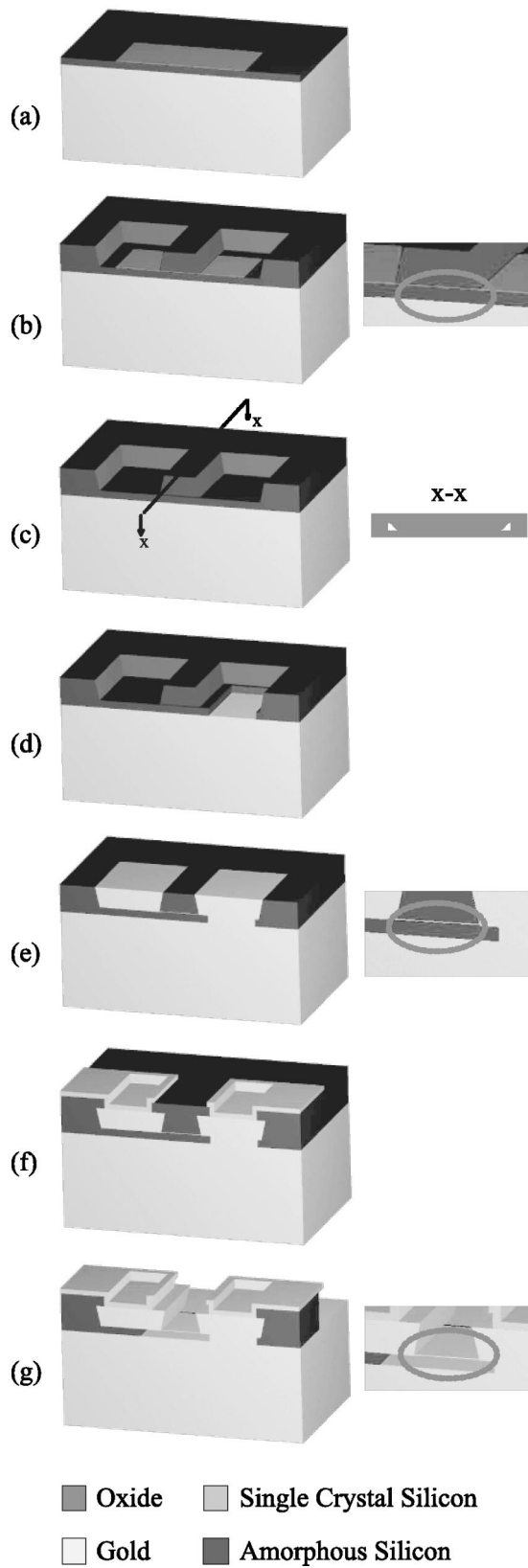[a]Electronic mail: bashir@ecn.purdue.edu

FIG. 1. Cross sections at various steps of the fabrication process. (a) Amorphous silicon sacrificial layer definition. (b) Etch of vias in the oxide to remove the sacrificial layer and define source/drain regions. Note the wires are defined by the thickness of the sacrificial layer. (c) Removal of the sacrificial layer and collapse of top oxide leaves a mold for the growth of wires. (d) Seed window etch down to the silicon substrate. (e) Polished surface after epitaxial growth. (f) Metal definition. (g) Release of the wires by blanket wet etching the encapsulating oxide layer in hydrofluoric acid.
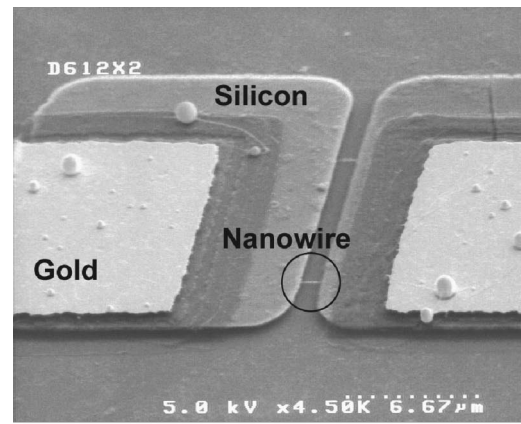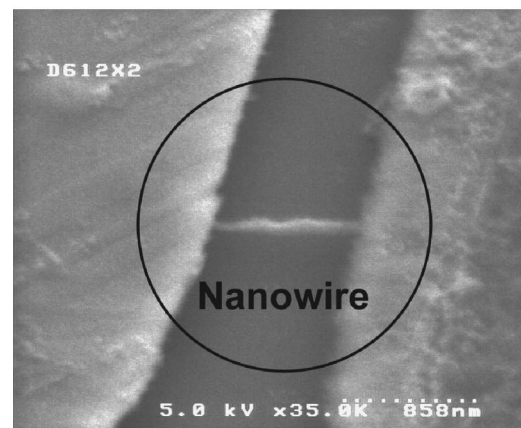
FIG. 2. Field emission scanning electron microscopy photos of the fabricated devices. (a) Zoomed out, showing the gold contacts, silicon source/drain islands and formed wires between the silicon islands. (b) Zoomed in to the silicon wire.

device, leaving the plate and wires in place, with a supporting oxide layer below. A longer BHF etch (14 min) removes all remaining oxide as well as the thin silicon film between the wires, resulting in the formation of suspended nanowires. After rinsing, the samples were soaked in methanol without drying to ensure the complete displacement of the water, and then air dried. A scanning electron micrograph of a completed device is shown in Fig. 2.

Experiments were performed on both the plate and wire structures in order to verify the feasibility of using the structures as field effect sensors. While fluidic detection of chemical and biological analytes is the eventual goal for these devices, gas phase measurements were initially performed due to simpler experimental setup. All measurements were performed in a closed chamber where the ambient gas composition and pressure was controlled. A 1 kHz 10 mV peak-to-peak sinusoidal probe signal superimposed on a variable dc bias was produced by a function generator (Stanford Research Systems model DS345) and fed into the source electrode of the device. The resulting drain current was amplified through a low-noise current preamplifier (Stanford Research Systems model SR570) and detected using a lock-in amplifier (Stanford Research Systems model SR850). Dry nitrogen
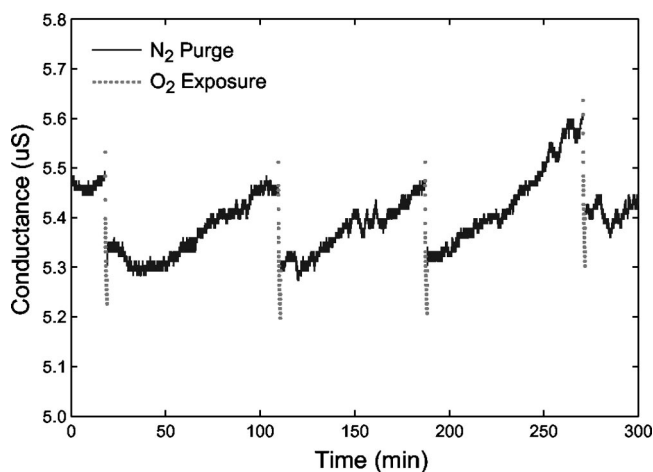
FIG. 3. Electrical response of the device upon exposure to oxygen (red dotted lines) and nitrogen (blue solid lines). Vertical axis shows the small signal conductance at 0 V dc bias and the horizontal axis the time in minutes. Experiment was performed at 82 °C of substrate temperature, and atmospheric pressure. Unlike nitrogen exposure, the conductance of the device decreases approximately 3% upon 1.5 min of exposure to oxygen. Note that the nitrogen purge steps recovers the oxygen sensitivity of the device.
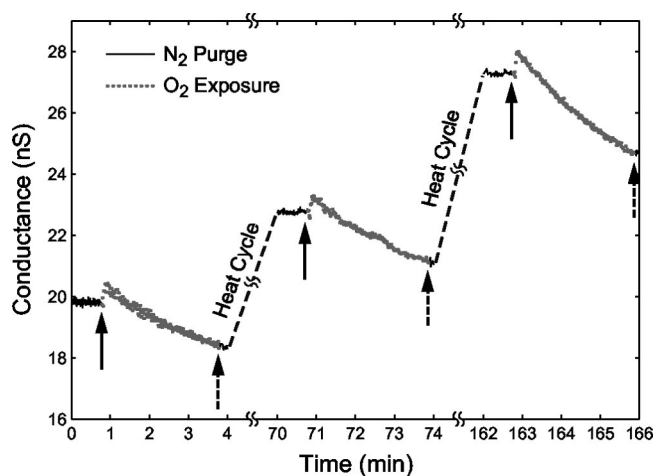

FIG. 4. Decrease in conductance of the silicon nanowire upon a 3 min exposure to oxygen/argon mixture shown in red dots (starting at solid arrow and ending at dashed arrow), largest decrease being 9%. Experiment was performed at 0 V dc bias, atmospheric pressure and room temperature. Devices were purged with nitrogen (blue solid lines) and heated in vacuum between subsequent oxygen exposures (dashed blue line) to recover the conductance.

was used to purge the test chamber, and 20% oxygen in argon was used as the analyte gas. Using the described setup, we were able to directly collect the small signal conductance (dI/dV) of the device as a function of time and dc bias. The effect of ambient gas on the conductance of the devices was investigated. As control measurements, we tested devices that were not released and found no reaction to oxygen ambient. Released devices exhibited up to a 9% decrease in conductance when exposed to 20% oxygen in argon.

We believe the decrease in conductance of the wire can be attributed to the physiosorption of oxygen species on the nanowire resulting in a decrease of the work function of the silicon surface. It is known that the work function of the silicon surface reduces upon exposure to oxygen, while it does not change upon exposure to inert gases.[6] A decrease in the work function will result in an increased energy barrier between the heavy doped *n*-type contact regions and the low doped wire, and result in a reduction of the current through the device. The oxygen molecule, which is a diradical and very reactive, effectively induces a net negative charge on the surface of the wires. This results in a net depletion of the silicon nanowire/native-oxide interface, causing an effective decrease of its electrical diameter. These hypotheses are confirmed by our measurement results. Control experiments were also performed on released devices with pure argon gas to ensure the conduction change was indeed due to oxygen. Devices which responded to the argon–oxygen mixture did not respond to pure argon.

It was also seen that the decrease in conductance was reversible and repeatable. Figure 3 shows a decrease in the conductance of the plate upon exposure to oxygen, and recovery of the conductance after purging in nitrogen. However, it can also be seen that the base line conductance of the device shifts for the same amount of recovery time, indicating some irreversibility of the adsorption. In order to fully recover the conductance of the devices, they were heated in

vacuum at elevated temperatures (80–90 °C). A similar set of experiments was also performed on the wire structures. The wire structures showed similar response to exposed oxygen, however, simply purging the test chamber was not sufficient to recover the conductance of the wire device. Device conductance continued to decrease at a slower rate after the nitrogen purge was started until the chamber was evacuated. After evacuation of the chamber the conductance stabilized at a constant value. In order to desorb the oxygen, the nanowire device was heated up to 80 °C in vacuum and cooled back to room temperature. Upon this procedure the device conductance increased due to desorption of oxygen gas from the wire surface. A device cycling experiment is shown in Fig. 4.

The results obtained from gas phase measurements are very encouraging, and suggest that the use of a top-down nanofabrication technique is capable of producing nanoscale sensors for the detection of very low concentrations of analytes. By analyte specific receptors or ligand functionalizing and placement of these sensors in a microfluidic channel, highly specific and high throughput analysis systems can be realized in a well-integrated fashion. Such work is currently underway and will be reported when complete.

[1] K. Besteman, J. L. Lee, F. G. M. Wiertz, H. A. Heering, and C. Dekker, Nano Lett. **3**, 727 (2003).
[2] Y. Cui, Q. Wei, H. Park, and C. M. Lieber, Science **293**, 1289 (2001).
[3] J. F. Klemic, E. Stern, and M. Reed, Nat. Biotechnol. **19**, 924 (2001).
[4] Y. K. Choi, T. J. King, and C. Hu, IEEE Electron Device Lett. **23**, 25 (2002).
[5] P. J. Schubert and G. W. Neudeck, IEEE Electron Device Lett. **11**, 181 (1990).
[6] K. Nakayama and L. Zhang, Jpn. J. Appl. Phys., Part 1 **39**, 4509 (2000).